



www.sciencemag.org/cgi/content/full/332/6036/1410/DC1

Supporting Online Material for

**Direct Observation of Nodes and Twofold Symmetry in FeSe
Superconductor**

Can-Li Song, Yi-Lin Wang, Peng Cheng, Ye-Ping Jiang, Wei Li, Tong Zhang, Zhi Li,
Ke He, Lili Wang, Jin-Feng Jia, Hsiang-Hsuan Hung, Congjun Wu, Xucun Ma,*
Xi Chen,* Qi-Kun Xue

*To whom correspondence should be addressed. E-mail: xcma@aphy.iphy.ac.cn (X.M.);
xc@mail.tsinghua.edu.cn (X.C.)

Published 17 June 2011, *Science* **332**, 1410 (2010)
DOI: 10.1126/science.1202226

This PDF file includes:

Materials and Methods
Figs. S1 to S6
References

Supporting Online Materials for

“Direct Observation of Node and Two-Fold Symmetry in FeSe Superconductor”

Can-Li Song^{1,2}, Yi-Lin Wang², Peng Cheng¹, Ye-Ping Jiang^{1,2}, Wei Li¹, Tong Zhang^{1,2}, Zhi Li²,
Ke He², Lili Wang², Jin-Feng Jia¹, Hsiang-Hsuan Hung³, Congjun Wu³, Xucun Ma^{2,*}, Xi Chen^{1,*},
and Qi-Kun Xue^{1,2}

* To whom correspondence should be addressed. Email: xcma@aphy.iphy.ac.cn,

xc@mail.tsinghua.edu.cn

This supplement contains:

Materials and Methods

Figs. S1 to S6 and captions

References

This file is in Word format.

Materials and Methods

The experiments were conducted in an ultrahigh vacuum low temperature (down to 0.4 K) STM system equipped with a molecular beam epitaxy (MBE) chamber for film growth. The base pressure is better than 1×10^{-10} Torr. The graphitized SiC(0001) substrate mainly consists of double-layer graphene, prepared using the well-established recipe (Ref. S1). During film growth, high purity Fe (99.995%) and Se (99.999%) at a nominal Se/Fe beam flux ratio of ~ 20 were co-deposited onto the graphitized SiC(0001) substrate held at 450°C. The high flux ratio compensates the losses of volatile Se molecules and leads to atomically flat and stoichiometric FeSe samples. The excess Se will desorb and cannot be incorporated into the stoichiometric FeSe film due to the high substrate temperature. The lowest density of Se vacancies, typically one in an area of $100 \times 100 \text{ nm}^2$ (\sim one per 70000 Se sites), was found on the surface.

Se-rich $\text{Fe}_{1-x}\text{Se}_{1+x}$ samples (x refers to the doping level in the top Se-Fe-Se layer) were prepared by doping extra Se into the stoichiometric FeSe samples held at 220°C. We found that the superconductivity was completely destroyed at a doping level of approximately $x = 0.025$ (fig. S5). Further Se doping induces $\sqrt{5} \times \sqrt{5}$ superstructure on the surface. The extra Se atoms can be removed by annealing the Se-rich samples at 450°C. In this case, the superconductivity is recovered.

To reveal the superconductivity behavior of the FeSe samples, special measures such as grounding and shielding were taken to increase the stability and spectroscopic resolution of our STM system (Ref. S2). In all STM/STS measurements, a polycrystalline PtIr tip was used. The STS and dI/dV maps were acquired using lock-in technique with a bias modulation of 0.1 mV at 931 Hz. The pixels for all STM topographic images are 512×512 , while the pixels for all dI/dV maps are 64×64 . The STM images were processed using WSxM software (Ref. S3).

S1. J. Hass *et al.*, *J. Phys.: Condens. Matter.* **20**, 323206 (2008).

S2. S. H. Ji *et al.*, *Phys. Rev. Lett.* **100**, 226801 (2008).

S3. I. Horcas *et al.*, *Rev. Sci. Instrum.* **78**, 013705 (2007).

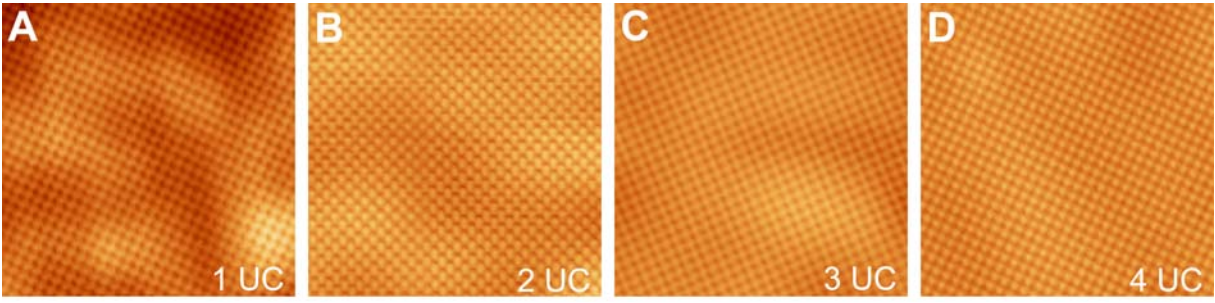


Fig. S1. (A-D) Atomically resolved STM topographic images ($V = 10$ mV, $I = 0.1$ nA, 10×10 nm²) taken on the FeSe film with a thickness of 1, 2, 3 and 4 unit cells (UC), respectively. All the films show a defect-free surface.

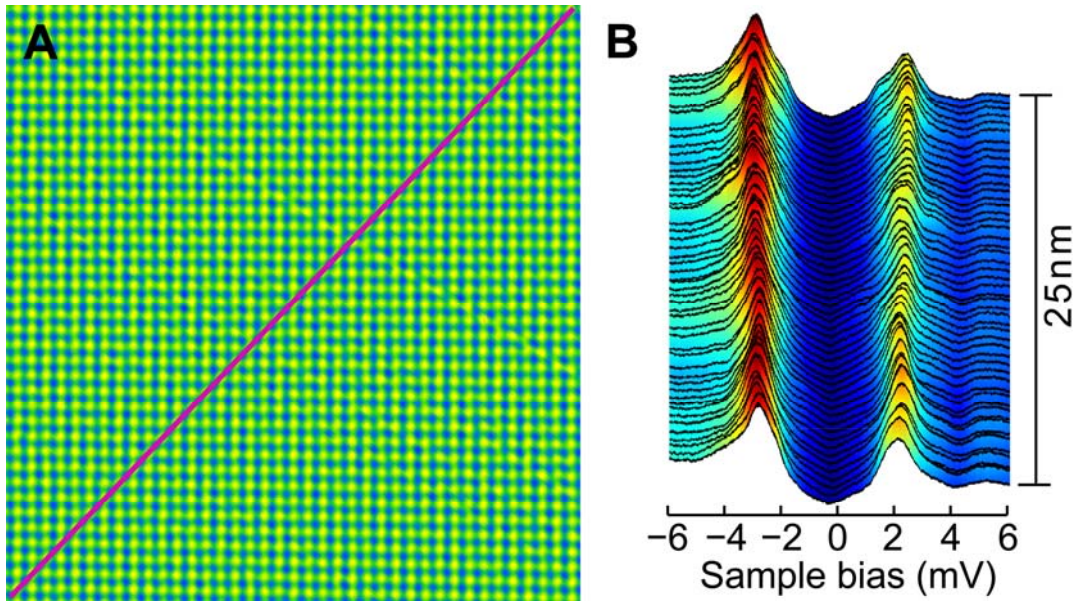


Fig. S2. The uniformity of the superconducting gap of FeSe. **(A)** A typical topographic image of our FeSe samples. The size of the image is $20 \times 20 \text{ nm}^2$. **(B)** A series STS spectra showing spatial homogeneity of the superconducting gap in our FeSe samples prepared by MBE. The spectra were measured along the purple line in (A). The tunneling conditions: $V = 10 \text{ mV}$ and $I = 0.1 \text{ nA}$.

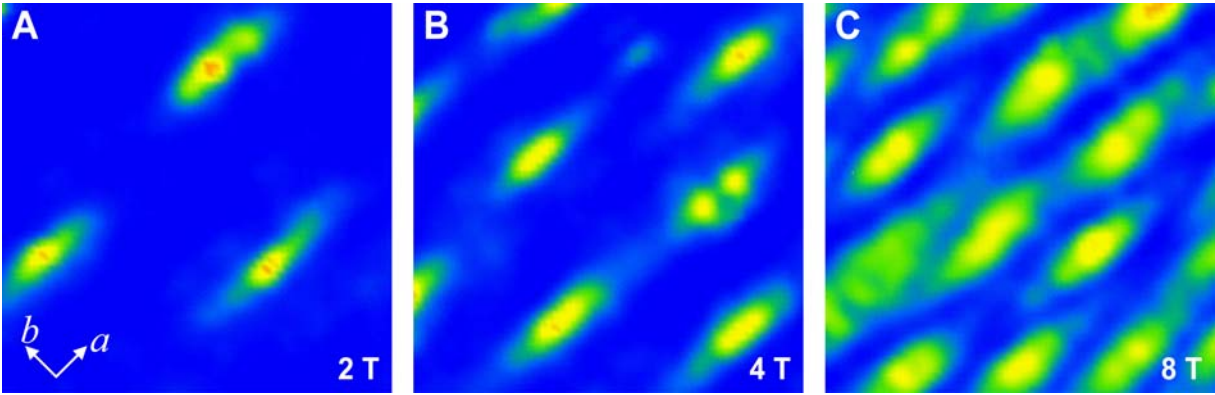


Fig. S3. Magnetic field-dependent vortex lattices. The images from (A) to (C) show the zero bias conductance maps at 0.4 K under a magnetic field of 2, 4 and 8 Tesla, respectively. In the images, all vortices (the bright features) show elongated shape along the a -axis. At high field (8 Tesla) in (C), the vortices arrange into a distorted hexagonal Abrikosov lattice. The image size is $60 \times 60 \text{ nm}^2$. Setpoint: $V = 10 \text{ mV}$, $I = 0.1 \text{ nA}$.

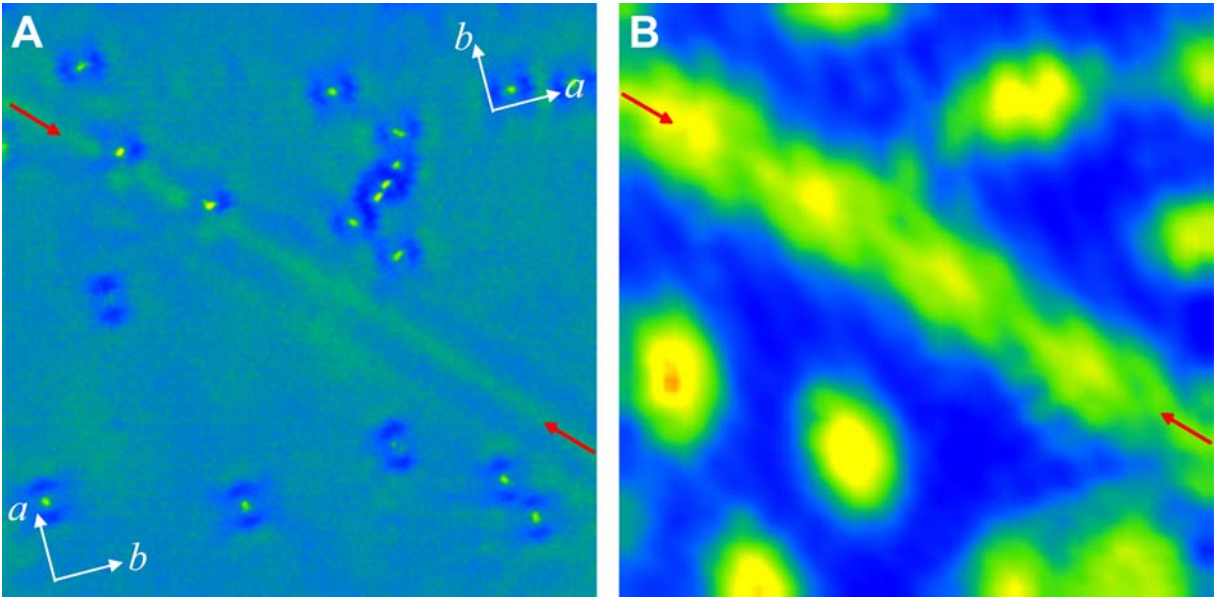


Fig. S4. (A) STM topography ($V = 10$ mV, $I = 0.1$ nA, 100×100 nm²) and (B) the simultaneously measured zero bias conductance map at 2 Tesla and 4.5 K. The surface was doped with extra Se atoms, which substitute the second-layer Fe, as discussed in fig. S5. The red arrows indicate the domain boundaries. The crystallographic orientations of the two neighboring domains are orthogonal. The vortex orientation is rotated by 90° across the boundary.

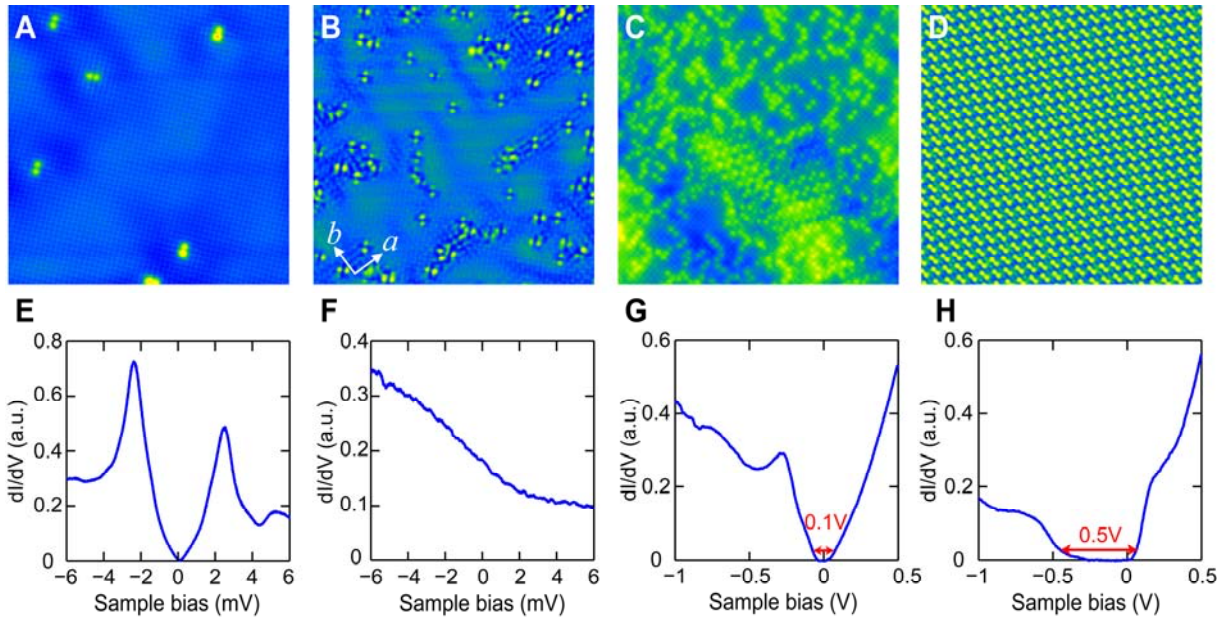


Fig. S5. STM topography ($V = 10$ mV, $I = 0.1$ nA, 20×20 nm²) and electronic structure of Fe_{1-x}Se_{1+x} with different Se doping level (x). (A) $x = 0.001$, (B) $x = 0.025$, (C) $x = 0.049$, (D) $x = 0.1$. The Se-terminated 1×1 surface is very stable and individual Se atoms don't adsorb on the surface at 220°C. It suggests that the extra Se atoms seen in (A) do not stay on the top of FeSe surface, but instead they substitute the subsurface Fe atoms. Because there are two distinctive substitution sites, the dumbbell-like feature appears with two perpendicular orientations. Similar to Fig. 4, the quantum interference pattern can be seen in (B). (E-H) Tunneling conductance spectra on the surface shown in (A-D), respectively. The spectrum in (E) was taken at a location away from the extra Se dopants, while the spectra in (F), (G) and (H) were spatially averaged. The superconductivity is completely suppressed at $x = 0.025$ (F). Further increase of the Se composition leads to semiconducting behavior with an asymmetric gap near E_F (G). The extra Se atoms are ordered into $\sqrt{5} \times \sqrt{5}$ superstructure with a large energy gap of ~ 0.5 eV at very high concentration of Se (H).

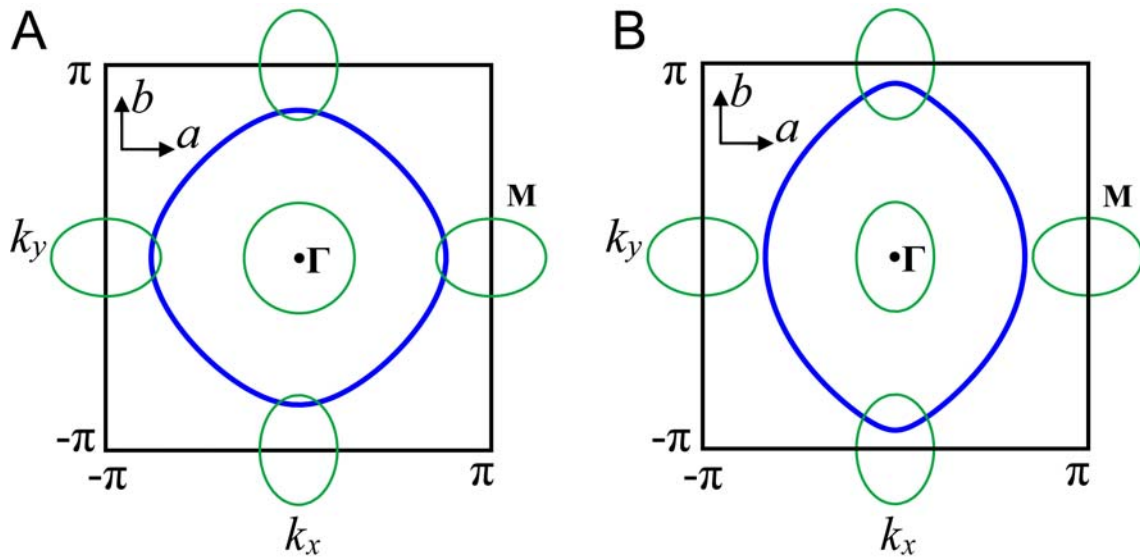


Fig. S6. Nodal lines for different degrees of anisotropy. The ratio between Δ_1 and Δ_2 is 0.35. The observations of broken C_4 tetragonal symmetry suggest the orbital-dependent reconstruction of the electronic structure. The direct consequence is that the interactions between the hole pocket and the electron pockets at $(0, \pm\pi)$ and $(\pm\pi, 0)$ points are nonequivalent. This effect breaks the four-fold rotational symmetry of the gap function, which can be roughly taken into account by modifying Eq. (1) into $\Delta_{s\pm} = \Delta_1 \cos k_x \cos k_y + \Delta_2 (\cos k_x + \lambda \cos k_y)$. **(A)** The nodal line in the case of the 4-fold symmetry ($\lambda = 1$). The nodal lines are distorted from the diamond box in Fig. 1D. The four vertices of the diamond are smoothed and move away from the M-points $(\pm\pi, 0)$ and $(0, \pm\pi)$. **(B)** The nodal line with further breaking of the four-fold symmetry ($\lambda = 0.7$). The nodal line is pushed away from the M-points of $(\pm\pi, 0)$, and the nodes disappear on the horizontal electron pocket. On the other hand, the nodal line is pushed back toward the M-point of $(0, \pm\pi)$, and the nodes remain on the vertical electron pocket. Therefore, the anisotropic electronic structure can lead to the removal of nodes along the b -axis. The values of Δ_1/Δ_2 and λ are arbitrarily chosen to discuss the mechanism.